Effective Charges Near 56Ni and Production of Anti-Nuclei Studied with Heavy-Ion Reactions

du Rietz, Rickard

2005

Citation for published version (APA):
du Rietz, R. (2005). *Effective Charges Near 56Ni and Production of Anti-Nuclei Studied with Heavy-Ion Reactions*. [Doctoral Thesis (compilation)]. Intellecta DocuSYS AB.

Total number of authors:
1

Paper I

ELSEVIER
Available online at www.sciencedirect.com
SCIENCE DIRECT®
Nuclear Instruments and Methods in Physics Research A 497 (2003) 263–293
NUCLEAR INSTRUMENTS & METHODS IN PHYSICS RESEARCH
Section A
www.elsevier.com/locate/nima

Construction and performance of the PHENIX pad chambers

K. Adcox[a], J. Ajitanand[b], J. Alexander[b], J. Barrette[c], R. Belkin[d], D. Borland[a], W.L. Bryan[e], R. du Rietz[f], K. El Chenawi[a], A. Cherlin[g], J. Fellenstein[a], K. Filimonov[c,1], Z. Fraenkel[g], D. Gan[c,2], S. Garpman[f,✠], Y. Gil[g], S.V. Greene[a], H.-Å. Gustafsson[f], W. Holzmann[b], M. Issah[b], U. Jagadish[e], R. Lacey[b], J. Lauret[b,d], W. Liccardi[d], S.K. Mark[c], J. Milan[b], T.E. Miller[a], A. Milov[g,3], J.T. Mitchell[d], P. Nilsson[f,4], L. Nikkinen[c], J. Nystrand[f], E. O'Brien[d], A. Oskarsson[f,*], L. Österman[f], I. Otterlund[f], Y. Qi[c,5], B. Pasmantirer[g], C. Pinkenburg[b,d], I. Ravinovich[g], M. Rosati[c,6], A. Rose[a], D. Silvermyr[f,7], M. Sivertz[d], M.C. Smith[e], N. Starinsky[c,8], E. Stenlund[f], O. Teodorescu[c,9], I. Tserruya[g], H. Tydesjö[f], W. Xie[g,10], G.R. Young[e], V. Yurevich[g,11]

[a] *Vanderbilt University, Nashville, TN 37235, USA*
[b] *Chemistry Department, State University of New York - Stony Brook, Stony Brook, NY 11794, USA*
[c] *McGill University, Montreal, Que., Canada H3A 2T8*
[d] *Brookhaven National Laboratory, Upton, NY 11973-5000, USA*
[e] *Oak Ridge National Laboratory, Oak Ridge, TN 37831, USA*
[f] *Department of Physics, Lund University, Box 118, SE-221 00 Lund, Sweden*
[g] *Weizmann Institute of Science, Rehovot 76100, Israel*

Received 5 September 2002; accepted 10 September 2002

Abstract

We present the Pad Chamber detector system in the PHENIX experiment at the Relativistic Heavy Ion Collider (RHIC) at Brookhaven National Laboratory. The three station system provides space points along each track in the

---

*Corresponding author. Tel.: +46-46-222-0000; fax: +46-46-222-4015.
E-mail address: anders.oskarsson@kosufy.lu.se (A. Oskarsson).

[1] Present address: Lawrence Berkeley Nat. Laboratory, Berkeley, CA 94720, USA.

[2] Present address: Dept. of Electrical Engineering, Cornell University, Ithaca, NY 14853-7501, USA.

[✠] Deceased.

[3] Present address: State University of New York-Stony Brook, Stony Brook, NY 11794, USA.

[4] Present address: CERN, EP-division, CH-1211 Geneva 22, Switzerland.

[5] Present address: Dept. of Biomedical Engineering, University of North Carolina, Chapel Hill, NC 27599, USA.

[6] Present address: Iowa State University, Ames, IA 50011, USA.

[7] Present address: Los Alamos National Laboratory, Los Alamos, NM 87545, USA.

[8] Present address: Dept. of Physics and Astronomy, Queen's University, Kingston, ON, Canada K7L 3N6.

[9] Present address: Dept. of Computer Science, Cornell University, Ithaca, NY 14853-7316, USA.

[10] Present address: University of California-Riverside, Riverside, CA 92521, USA.

[11] On leave from the Joint Inst. for Nuclear Res. JINR, Moscow.

PII: S0168-9002(02)01791-6

spectrometer arms at mid-rapidity and covers a total area of 88 m^2. Its main functions are to provide the track coordinate along the beam and to ensure reliable pattern recognition at very high particle multiplicity. A new concept for two dimensional wire chamber readout via its finely segmented cathode was developed. The full readout system, comprising 172 800 electronic channels, is described together with the challenging design of the chambers. The electronics, mounted on the outer chamber face, together with the chamber itself amounts to 1.2% of a radiation length. Results from cosmic ray tests, showing an average efficiency better than 99.5% for all chambers are presented. The experiences from the full scale operation in the first run are reported.

PACS: 29.40.CS; 29.40.GX

Keywords: PHENIX; RHIC; Tracking; Wire chamber; Cathode pixels; Readout electronics

---

1. Introduction

Collider experiments with beams of heavy nuclei at very high energy, are now possible at the Relativistic Heavy Ion Collider (RHIC), at Brookhaven National Laboratory, and in the future at the Large Hadron Collider (LHC) at CERN. Heavy ion collisions, introduce additional experimental challenges compared to collider experiments with protons. Whereas the luminosities with heavy ions are low (at best $10^{27}\ s^{-1}/cm^{-2}$), the number of charged particles emitted per central Au–Au collision is about 4800 at the highest RHIC energy [1–3] and may be as large as 50 000 at LHC. At the time of design of the RHIC experiments, the expected multiplicities ranged up to a factor two larger than what has now been measured.

Detector systems, aiming at observing individual particles under such conditions must cope with the high multiplicities by using a very fine granularity to reduce the occupancy. The large channel count makes it necessary to place the amplifying and digitizing electronics in specialized integrated circuits, on the detector. Transfer of digitized data from the detector profits from advances in broadband technology, allowing serial transfer from a large number of channels via fiber optic links.

This paper describes the design, construction, testing and performance of the Pad Chambers which form part of the particle tracking system at mid rapidity of the PHENIX detector [4,5]. Three layers of Pad Chambers define three space points along the straight line tracks through the tracking spectrometers which also include specialized detectors for momentum and particle identification.

2. The PHENIX experiment

The main objectives of the PHENIX experiment at RHIC are to measure rare observables like leptonic decays of light (ω, ρ, ϕ) and heavy $(J/\Psi, \Psi'$ and $\Upsilon)$ vector mesons and phenomena at high p_T, all requiring maximal collision rate. PHENIX is thus only using tracking detectors with short drift times. The leptonic decays are observed in the $\mu^+\mu^-$ channel at large rapidity and in the e^+e^- channel at mid-rapidity.

The PHENIX detector is built (Fig. 1) around a central, circular dipole magnet with a vertical gap producing a radially varying axial field with about 2 m radius. Two spectrometer arms, named east and west, located in the field free region, view the collisions from opposite sides. The arms cover the mid-rapidity region $|\eta| < 0.35$, each one with a 90° coverage in azimuth. The arms are positioned with a 67.5° opening at the top (and 112.5° at the bottom) rather than 90° both up and down, in order to obtain a finite acceptance for all relative azimuthal angles within particle pairs and thus a smooth acceptance in transverse momentum for the parent particles.

Several stations of tracking detectors (Fig. 2), including the Pad Chambers are complemented by a Ring Imaging Čherenkov detector (RICH) and an Electromagnetic Calorimeter (EMCal) for

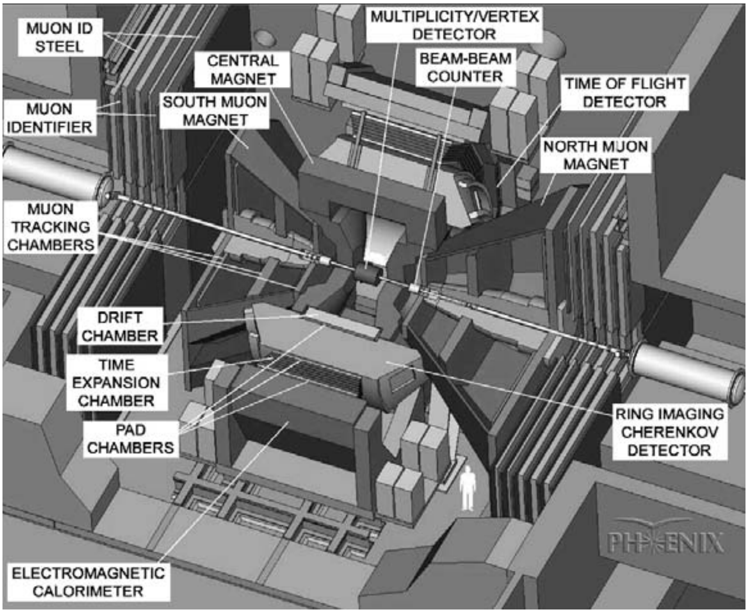

Fig. 1. The baseline PHENIX detector.

electron identification and photon detection. Hadron identification is possible in the full aperture by time of flight measurements using the good time resolution of the calorimeters. In addition, specialized high resolution Time-of-Flight (TOF) detectors cover a subset of the mid-rapidity acceptance. The start time is determined by the Beam–Beam Counters (BBC), which also provide a coarse determination of the vertex position.

Conically shaped magnets surround the beams in the forward and backward directions, forming radial magnetic fields for the muon tracking spectrometers which end with muon identifiers. The muon detection is less affected by the large number of produced hadrons since these are absorbed in the iron of the central magnet.

Three detector systems characterize the collisions with regards to global properties related to the impact parameter. The signal from the BBC reflects the particle density at large pseudorapidity ($3.1<|\eta|<3.9$). The MVD (Multiplicity and Vertex Detector), close to the vertex, measures the multiplicity ($|\eta|<2.6$) and the interaction coordinate, while the dual Zero Degree Calorimeters (ZDC) view the collision along a tangent through the interaction region, thus integrating the non-interacting energy carried by single spectator neutrons.

2.1. The central arms

The design of the spectrometer arms at mid-rapidity was driven by the strict requirements of electron identification, arising from the expected ratio of 10^3 or larger between the number of hadrons and electrons. Another mandatory concern was to reduce the photon conversion by pair production in various materials in the spectrometer, i.e. to minimize the radiation thickness of the detectors. The main source of high energy photons is π^0 decay and such photons are almost as numerous as charged hadrons.

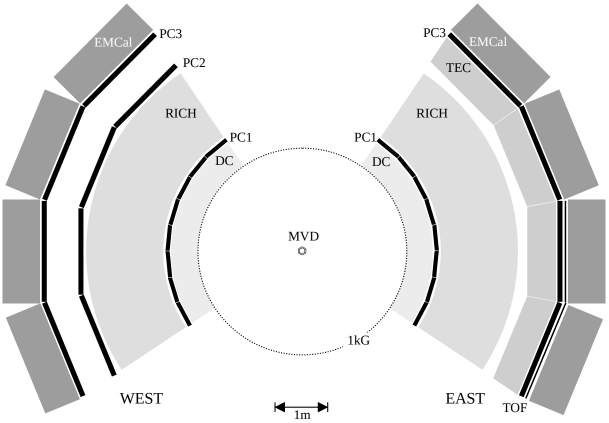

Fig. 2. A schematic illustration of the two mid-rapidity spectrometer arms. The cut is made by a plane, perpendicular to the beams, through the average collision point at the center of the magnet gap. The dotted circle represents the radius at which the magnetic field is approximately 1 kG which is about $\frac{1}{10}$ of the central field strength at the full field setting.

The main detector system (Fig. 2) for electron identification is the RICH (Čherenkov threshold). The momentum is obtained from the Drift Chambers (DC). Combining the momentum with the information from the EMCal (measured energy and flight time) and/or the Time Expansion Chambers (TEC) provides additional electron identification in certain momentum ranges.

All these means of identification are needed to obtain the required hadron rejection factor of 10^4 over a wide momentum range. This condition requires however that no errors are made when correlating the momentum measured in the DC placed between 2.0 and 2.5 m from the interaction region with the identifying information obtained at twice that distance. This means that a track has to be followed with very high reliability from detector to detector through the whole spectrometer, and this has to be achieved when several hundred particles pass through a spectrometer arm in a central collision. Reliable pattern recognition is the most important role of the Pad Chamber (PC) detector system.

The mid-rapidity spectrometers as they are visualized in Fig. 1, with the east and west arm tracking detectors being identical, was the original design. This plan was changed due to financial reasons, and the spectrometer arms have a TEC only in the east arm and PC2 only in the west arm as shown in Fig. 2. The mechanical design however, still allows the original version to be implemented.

2.2. Specifications of the Pad Chambers

As part of the requirements of the tracking system in the PHENIX central arms, the Pad Chambers must fulfill the following roles and have the following specifications:

- Provide reliable track information with accurate coordinate in the z direction (parallel to the beams) and good position resolution in the other (ϕ) direction.
- Provide redundancy for the drift chamber measurements (though with poorer azimuthal resolution).
- Very high detection efficiency.
- Low occupancy of individual channels.
- Define entry and exit coordinates of the particle identification subsystems, mainly the TEC, RICH and the EMCal.

- Minimum radiation thickness to minimize conversions.
- Provide fast position information to be used as input to the second-level trigger.

For a detector system, covering almost 100 m^2 in a cylindrical geometry, wire chambers with 2-dimensional cathode readout, are best suited to obtain the required functions of the Pad Chambers.

The DC and the TEC determine the track coordinate in the plane perpendicular to the beams (r–ϕ) with high resolution. Several close points are measured and the information can be put together to determine direction vectors in r–ϕ. This information alone would lead to combinatorial ambiguities when tracing particles through the spectrometer, i.e. connecting distant points, when the multiplicity is high. Another complication is that the occupancy of these systems is fairly high in the most central collisions.

Reliable pattern recognition through the spectrometer requires resolving the tracks in three dimensions. The three layers of Pad Chambers, located at the radial distances of 2.5 m (PC1), 4.2 m (PC2) and 4.9 m (PC3) from the interaction region, serve this purpose. Since they provide the coordinates of three space points on each track, the Pad Chamber information defines reliably the straight line particle tracks in the field free region. The transverse coordinates do not need to be precise, since the transverse momentum is determined by the DC.

The DC has some of the wires oriented at a small stereo angle (i.e. a small angle relative to the beam) providing a measurement also of the z-coordinate. However, the small stereo angle, the low number of wires and the high occupancy makes this z-measurement less reliable. The z-measurement provided by PC1 (placed immediately behind the DC), is thus the most accurate measurement of the z-coordinate, in particular at high multiplicity. To fulfill this crucial role in the tracking, the highest possible detection efficiency is required.

Tracking simulations, at the charged particle multiplicity expected in central Au + Au collisions, motivate an angular resolution in ϕ corresponding to a wire spacing in the pad chambers (at the PC1 position) of approximately 8 mm. Tentatively this results in a position resolution across the wires of $8/\sqrt{12} = 2.3$ mm. From the point of view of pattern recognition one would require to the same resolution along the wire (z). This z-resolution also satisfies the minimum requirements imposed by parallel momentum measurements and invariant mass reconstruction, which both are important measurements at the PC1 location. Reliable matching of tracks throughout the spectrometer motivates the same angular resolution for PC2 and PC3 as for PC1. Thus a doubled position resolution is acceptable for PC3, situated at approximately the double radial distance compared to PC1.

PC2 and PC3 also fulfill important roles in some of the particle identification sub-systems. For example, PC3, placed in front of the EMCal, allows tagging of charged particles entering the EMCal.

A mandatory concern was also to minimize the radiation thickness of the chambers, in particular PC1, in order to reduce the number of electron–positron pairs from conversion of high energy photons. Conversions further out can be eliminated in the offline analysis since these electrons cannot be traced back to the DC. Such electrons can however be a complication for the online electron trigger.

3. Pad readout of wire chambers

Two-dimensional readout of wire chambers is normally done by using a cathode segmented into readout pads. Different types of cathode segmentation have been used, such as the cathode strip chamber in which narrow strips are oriented at an angle relative to the wire [6], or the interpolating pad chamber [7] which uses Chevron shaped pads. Both solutions provide very good position resolution along the wire if the signal is spread over several pads/strips. For the tracking system in PHENIX, it was found that the granularity needed to master the high multiplicities made these types of solutions less suitable.

Instead, a new scheme for 2-dimensional readout of wire chambers was developed, based on readout cells having a size similar to the required position resolution. The simplest digital readout, i.e. just comparing the signal with a discriminator threshold, would then be adequate to meet the requirements on position resolution and one would have a system with very low occupancy, due to the fine granularity.

3.1. The pad geometry

A short presentation of the principles of the cell readout is given. Consider a detector with a square shaped readout cell with side w, i.e. a wire chamber with a wire spacing of w and anode–cathode distance of $w/2$. This would potentially result in a position resolution of $w/\sqrt{12}$ (the standard deviation of a rectangular distribution with total width w) across the wires. Along the wire a somewhat better resolution can be expected due to the continuous position sensitivity. The discussion can be generalized to any cell size as long as the ratio between cell width and anode–cathode distance is kept constant.

A straightforward segmentation of the cathode into $8 \times 8\ \mathrm{mm}^2$ sensor cells (as needed for the required position resolution in PC1) with an electronic readout channel connected to each, leads to such a low occupancy that it is not economically justified. Thus we adopt a pad geometry which effectively saves a factor 3 in the number of electronic channels while maintaining the position resolution of the original cell size $8 \times 8\ \mathrm{mm}^2$. The basics of the concept are described in Fig. 3.

3.2. The principle

The size of the cell is shown in Fig. 3a. Assume that we make three separate layers of pad chambers (individual wire chambers) each with the pad size equal to 3×3 cells. By shifting the three layers by one cell relative to each other in both dimensions, one would be able to reconstruct in which cell the hit is, since each cell means a unique combination of a hit pad from each of the three layers (Fig. 3b). In Fig. 3c, each pad has been cut into nine parts, called pixels, one in each cell covered by the pad, such that the three planes of pixels can be projected onto one single plane without any geometrical overlap. Since the avalanche (i.e. the signal) is always located on a wire, the sharing of the charge between the three pixels in the cell is only governed by the pixel geometry. The width of a pixel is thus chosen such that the same amount of charge is sensed, irrespective of the location of the pixel (position R, M or L) relative to the wire. Hence the pixel in position M (centered over the wire) has the smallest area while the pixels in positions R and L, located symmetrically with respect to the wire, have equal (and slightly larger) area. In panel Fig. 3d, the electrical connections between the nine pixels of a pad have been added.

The three layers of pads can thus be printed on one plane and this plane constitutes one cathode of a wire chamber. A pad is part of nine cells, but

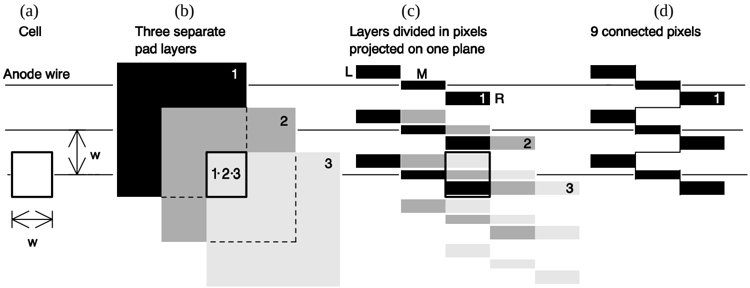

Fig. 3. Principles of the pad geometry.

since three pads are present in each cell, we have a reduction in the number of channels by a factor 3 compared to a system where each cell is a pad, read out by its own electronic channel. While retaining the position resolution of such a system, the staggered structure results in poorer double hit resolution.

This pad structure exhibits some other very advantageous features. The most important one is that a valid hit will always be sensed by three adjacent pixels belonging to three different pads. Since the charge sharing between the three pads is ruled by geometry and we have chosen the pixel area to collect equal fractions of the charge, we expect the requirement of triple registration to be fulfilled for every hit. Channels firing on electronics noise should thus be very unlikely to form false hits. Conventional discriminator based systems would have to operate at increased thresholds in order to avoid erroneous hits caused by electronic noise.

The function of a wire chamber, read out with this pad structure is fairly easy to simulate since the induced charge distribution on the cathode is well known [6]. Such simulations were done in the design phase and the simulations were verified with satisfactory agreement by studies of small prototype chambers [8]. The charge sharing on this pad structure was also studied analytically [9], and the successful agreement with experimental results, provided increased understanding of the readout concept.

The pad pattern, as it is actually etched is illustrated in Fig. 4. At the chamber edges, the pixels which would be outside the chamber are simply eliminated. Thus the readout and treatment of the information works identically at the edges as in the interior of the pad cathode.

3.3. Cell assignment algorithm

At first sight the pad pattern appears to be very complicated. To assign which cell has been hit

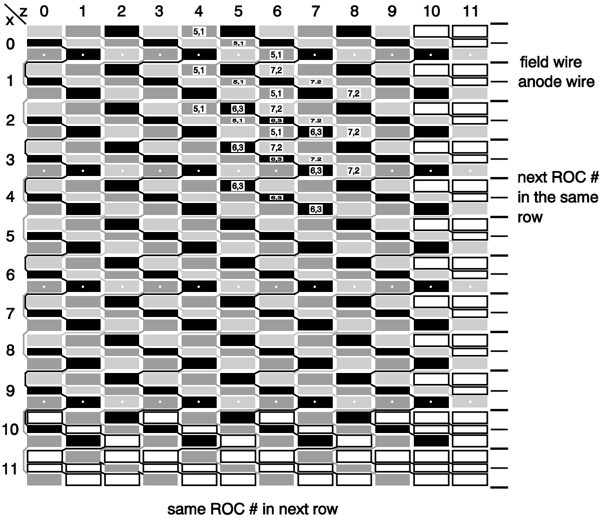

Fig. 4. The pad pattern of 48 pads handled by one readout card (ROC, cf. Section 5). The top and left edges illustrate how the pads are cut at the chamber edges. Unfilled pixels are read out by neighboring ROCs. The numbered pads are an example of three fired pads due to a hit in cell (6, 2) corresponding to the triplet of pixels belonging to pads (5, 1), (6, 3) and (7, 2). The numbering convention follows the description in Section 3.3.

from the observed pad triplet is however straightforward in software. Each cell is given a (z_c, x_c) coordinate, where z_c is the position along the wire and x_c is the wire number. Each pad also has a coordinate (z_p, x_p) which coincides with the coordinate of the cell located at the center of the pad. When the hit pattern is reconstructed from the information of fired pads, one has to move from pad-space to cell-space. To find out, in which nine cells a certain pad is present, is a trivial task, but to find out which three pads belong to a given cell is not as easy. A general transformation between pad space and cell space has the form:

$$z_p = z_c + \delta_z,$$
$$x_p = x_c + \delta_x$$

where δ_z and δ_x take the values -1, 0 or 1. If we number the three pixels of a cell 0, 1 and 2 (from top to bottom) a general expression is

$$z_p(i) = z_c + 1 - i$$

$$x_p(i) = x_c + (k - x_c \pm (i - z_c)) \bmod 3 - 1$$

for $i = 0$, 1 and 2. The two signs in the expression for x_p correspond to the two different possible orientations of the global pattern (the two mirror images). The value of k (either 0, 1 or 2) corresponds to the three possible different boundary conditions imposed by the plane edges, i.e. the pad configuration at the corner where the pattern starts. In this particular design, we have a + sign and the value of k is 0.

There is of course also a possibility to use the mirror image of an individual pad (or to look at the plane from the opposite direction). This, however, gives the same formulae if we instead count the i-value from bottom to top in each cell.

4. The wire chambers

This section describes the mechanical design and construction of the chambers using PC1 as an example. Specific features of PC2/3 are mentioned where they differ significantly from PC1. Table 1 summarizes the most important design parameters of the three chamber types.

4.1. Mechanical design

As indicated in Section 2, the basic requirements of the Pad Chambers are to achieve the highest possible efficiency and to minimize the amount of material used in the chamber construction. Both requirements are particularly important for PC1. In order to achieve the highest possible efficiency, dead or inactive areas due to frames etc., must be avoided. Thus a frameless construction was chosen for PC1, in which the wire tension is counteracted by the rigidity of honeycomb sandwich structures, building up the cathode planes.

Table 1
Design parameters of the individual chambers. The radiation thicknesses for PC2 and PC3 are for the sensitive area only

Parameter	PC1	PC2	PC3
Gas gap (mm)	6.0	10.0	12.0
Number of wires	58	116	116
Wire pitch (mm)	8.4	13.6	16.0
Length (cells)	212	106	106
Cell pitch (mm)	8.45	14.2	16.7
Dimensions L × W × H (cm)	198 × 50 × 6.0	151 × 157 × 7.2	177 × 185 × 9.0
Total weight (kg)	7	60	80
Maximal vertical sag (mm)	<1	<1	<1
FR4 thickness (mm)	0.25	0.75	0.75
Honeycomb thickness (mm)	24.5	32	38
Copper thickness (μm)	5	16	16
Radiation thickness (% X_0)	1.2	2.38	2.37
Dead area by design (%)	<0.7	7.6	7.6

The scale for the acceptable amount of material in PC1 is set by the Dalitz decay $\pi^0 \rightarrow e^+e^-\gamma$ which has a branching ratio of 1.2%. The goal of the PC1 design was to keep the photon conversion rate comparable to, or below, the Dalitz decay rate. The largest source of conversions would normally be the copper cladding (usually 36 μm thick) on each side of the (FR4 fiberglass) circuit boards. This is unacceptable and in cooperation with the manufacturer [10] the copper cladding was reduced to only 5 μm for the ($0.5 \times 2\ \mathrm{m}^2$) PC1 boards. The amount of glue used in the construction was carefully measured so as to minimize its contribution to the overall radiation budget of the chambers.

The boards with etched pixel pattern also have copper plated feedthrough holes bringing the signals to the opposite face of the board (named spider board due to the spider-like, etched trace pattern). The copper plating process would by standard methods add about 30 μm copper to each face of the board. After refining the plating process by the manufacturer [10], the additional copper deposit was reduced to 1–2 μm, with maintained quality of the electrical connection through the hole.

PC1 is subdivided into 2 × 8 sectors, each one with a trapezoidal profile in order to follow the arc shape of the Drift Chamber with a minimum of dead areas. Special care was taken in the tolerances of the global dimensions allowing the mounting of the 8 sectors on each of the two central arms with only 1 mm clearance between two adjacent sectors. Fig. 5 shows a vertical cut through a Pad Chamber and Fig. 6 shows an exploded view of the individual parts of PC1.

Each sector is an independent chamber 1974 mm long, 495 mm wide at the middle plane of the trapezoid and 58 mm thick. It is made out of two flat panels, the pixel panel and the cathode panel, and an anode wire electrode between them.

Each panel consists of two 0.25 mm thick FR4 facesheets glued to a 25.4 mm thick honeycomb core. The solid cathode panel has a copper layer on its inner side, which serves as ground electrode. Gas is fed through recesses made in the

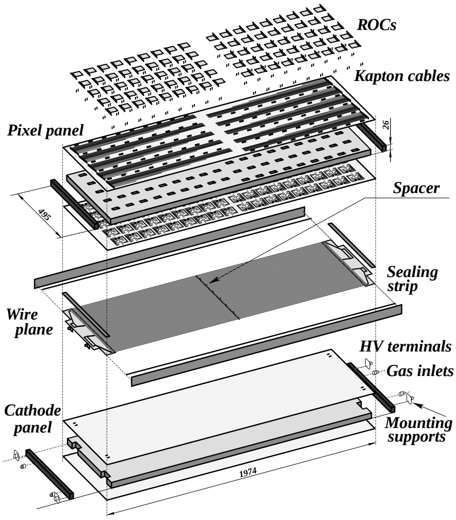

Fig. 6. Exploded view of a PC1 chamber.

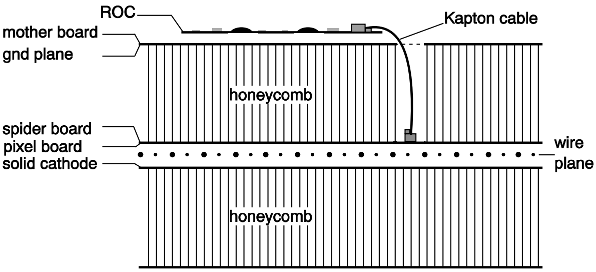

Fig. 5. Vertical cut through a chamber. Copper coated facesheet surfaces are named.

panel heads, the honeycomb and the facesheet to provide flow from one side of the detector to the other.

The two facesheets of the pixel panel are the pixel board and the motherboard. The pixel board is a double sided printed circuit board with the pixel pattern on its inner side (not visible in the sketch) and the signal traces on the other side. Approximately 4500 plated-through holes in each pixel board connect the pads to the traces. The traces are bunched in groups of 24 traces to a total of 180 microconnectors soldered to the ends of the traces. The signals are taken through the panel by flexible Kapton cables plugged into the microconnectors and the readout cards (ROCs) on the motherboard. See Section 5.

The motherboard has 2×5 signal busses on the outer side bringing the signals to and from the ROCs to the front-end electronic module (FEM) connected to the PHENIX DAQ by optical links. The inner side of the motherboard is copper clad to screen the signal traces from the noise coming from the communications in the busses. Several power lines on the motherboard were later reinforced with wires to reduce the resistivity along the 90 cm long traces made of very thin copper.

The anode wires are made of a tungsten–rhenium alloy with gold coating with a diameter of 25 μm. The field wires are gold-coated copper–beryllium of 75 μm diameter. The wire tension is 60 g for the anode wires and 120 g for the field wires, which is less than $\frac{2}{3}$ of their elastic limit. The spacing between the anode wires, the field wires and the anode-to-cathode gap for all chambers are given in Table 1.

The wires are glued and soldered to two terminal boards located at the edges of the chambers. The terminal boards distribute the high voltage through individual RC filters to each anode wire. The wires are grouped into four independent HV sectors limiting the loss to a part of a chamber in case of a broken wire. The wires are also glued on a 1 mm wide spacer bar located in the center of the chamber ("Spacer" in Fig. 6). The height of the bar is equal to half of the gas gap. The spacer holds the wires in position when the chamber sags due to its own weight. The sagitta of a PC1 chamber, freely supported at the four corners, is about 1 mm. The gravitational sag of the wires themselves is less than 80 μm. Another purpose of the spacer is to avoid possible electrostatic staggering of the wires.

As mentioned above, the PC1 sectors are sealed by gluing. This has the advantage of considerably reducing both the dead area and the amount of material. However the price we pay is that repairing a chamber, once sealed, is practically impossible. The sealing is ensured by gluing two 3 mm thick end beams to the two panels along the short sides. Along the long sides the chamber is sealed with a 6 mm high C-shape strip. In addition, this element plays an important role in holding the two panels together making them as a single mechanical unit. There is an additional 0.2 mm thick protective sealing strip running on both sides of the chamber covering the gap and the sides of the panels. This design gives the chamber sufficient mechanical rigidity while minimizing the thickness of the materials used for the construction. The radiation budget of the chamber, specified in Table 2, does not exceed 1.2% of a radiation length including the electronics. In part, this is achieved by moving the more massive parts of the chamber such as mechanical supports, gas fitting, and high voltage connections to the edges of the detector, outside of the PHENIX acceptance. The total inactive area of PC1 is 0.7% of the whole acceptance of a PHENIX central arm.

The large area to be covered by the PC2 and PC3 layers, requires very large chambers. The outer detector in the spectrometer, EMCal, is segmented in 22.5° sectors in ϕ compared to 11.25° for PC1. All detector systems outside the RICH (e.g. PC2/3), which is shaped like an arc, follow the sector geometry of EMCal. These chambers are divided in two separate halves at the median plane of the spectrometer (i.e. at $z = 0$).

For PC2 and PC3, the requirement of minimum mass is less crucial (since they are located after the RICH detector which provides the main electron identification). The chambers are also four times larger in area (about 2×2 m^2 for PC3). Thicker honeycomb sheets (32 mm for PC2 and 38 mm in PC3) in the panels provide enough mechanical rigidity to these large chambers. Also the

Table 2
PC1 radiation budget

PC1 element	Material	X_0	Thickness	Area (%)	Rad. length (%)
Traces	Copper	1.43 cm	5 μm	~40	0.014
Facesheet×4	FR4	17.1 cm	0.25 mm × 4	100	0.580
Screen	Copper	1.43 cm	5 μm	100	0.035
Glue joint×4	Epoxy	25 cm	~50 μm × 4	100	0.080
Panel core×2	Honeycomb	81.7 m	25.4 mm × 2	100	0.060
Traces	Copper	1.43 cm	5 μm	~10	0.005
Pads	Copper	1.43 cm	5 μm	~90	0.030
Wires	W/Au Cu/Be	0.35, 1.4 cm	25, 75 μm	0.3, 0.8	0.005
Gas	Air Ar/ethane	304, 165 m	2 × 25.6 mm	100	0.020
Cathode	Copper	1.43 cm	5 μm	100	0.035
Hole sealing	Epoxy	25 cm	~10 μm	100	0.005
Gap sealing	FR4	17.1 cm	6 mm	0.4	0.015
Sealing strip	FR4	17.1 cm	56 mm	0.08	0.025
Edge finish	Epoxy	25 cm	~40 μm	100	0.015
Solder joint	Pb/Sn/Flux	~1 cm	0.2 mm	1.4	0.028
Connectors	Nylon/brass	20 cm	~2 mm	—	0.080
Kapton cables	Kapton + copper	17 cm	Undefined	—	0.020
ROCs	Polyimid + comp.	18 cm	Undefined	30	0.110
Total			65 mm		1.16

FR4-fiberglass face sheets (760 μm) and the copper cladding (16 μm) were thicker compared to PC1. Most of the mechanical strength relies on honeycomb sandwich structures as for PC1. A thin frame construction housing an O-ring provides the gas seal.

PC2 is very similar to PC3 in design. The linear dimensions are however scaled down by approximately 0.85 due to the closer radial position of PC2. Of the two, PC3 was the most challenging to build due to the large size. Circuit boards of this size were too large to manufacture in one piece. However, a $1 \times 2\ \mathrm{m}^2$ board area was feasible and a square profile S2-glass tube with the same thickness as the honeycomb was used as a joint piece (along z) when gluing two circuit boards together to form the full plane. The etched pad pattern, was cut at the seam in the same way as at the chamber edges. The seam does not introduce any dead areas. In terms of data readout, PC2 and PC3 are segmented identically to PC1 and the same readout architecture and software treatment can be used all over the Pad Chamber system.

The board size needed for PC3-chambers proved to be at the limit of what was possible. Even after optimization of line spacing, line width and hole diameter, the manufacturing did not reach a quite predictable state and a careful testing and inspection was needed, followed by some repair by hand. The slightly smaller boards for PC2 had considerably fewer errors.

Around the edge of the honeycomb sandwich, a solid frame was glued. In the fiducial volume of the spectrometer it is as thin as possible. Bolts through the frames hold the pixel- and cathode panels together, pressing the panels against the O-ring seal. The edges of the chamber are cut at a right angle to the plane of the detector. The dead area imposed by the frames is 7.6% and coincides to a large extent with the sector edges of neighboring detector systems. Localized, thick material, like the frames, have proven by simulations to be acceptable at the radial positions of PC2 and PC3.

A thin wire support is placed along the pixel surface at the centerline of the chamber. Close to the center point of the chamber, the distance between the two panels is fixed by a small spacer and a nylon screw, preventing bulging due to the slight overpressure in the chamber.

The material thickness of PC2/3 is less critical than for PC1. The radiation thickness compares to the PC1 values as in Table 2 as follows: The contribution from copper is a factor 3.2 larger than on PC1 and a factor 3 larger from the FR4 facesheets. All other materials covering 100% of the area have about the same radiation thickness as on PC1. Materials with less than 100% coverage have a factor 2 to 4 lower radiation thickness than on PC1. This comparison applies to the sensitive parts of the detector. The frames, placed in insensitive parts have a considerable local thickness.

4.2. *Pixel board test*

A critical and challenging step before starting the construction of the chambers is the testing of the pixel boards. Once glued together with the honeycomb, repairs are practically impossible. The pixel electrode and signal transport to the ROCs form a complex structure: on the wire side it consists of 36 888 pixels connected into groups of nine pixels by narrow 150 μm wide copper traces (and similar minimum line spacing) forming 4320 pads. These connect to traces on the other side of the board by plated-through holes. These traces bring the signals to 180 microconnectors, one for each group of 24 pads. Flexible Kapton cables 36 mm long (41 mm on PC2 and 49 mm on PC3) transport the signals to microconnectors on the ROCs.

A trace pitch of this order is a challenge even on small boards and here it has to be etched, with uniform quality, on a $0.5 \times 2\ \mathrm{m}^2$ board. The twice as large boards for PC2/3 have only slightly larger minimum trace pitch and the need for board tests was as large as for PC1. The whole assembly of pixel board, microconnectors and Kapton cables must be checked for electrical conductivity from the pixel to the end of the Kapton cable and for shorts between neighboring traces. Standard tools are inadequate for this task. A reliable, efficient and fast test method was developed, together with the necessary tooling (including mechanics and a dedicated electronic unit) to test the pixel structure.

The tests consisted of: (i) ohmic connection, i.e. check electrical continuity from the pixels up to the end of the Kapton cable and (ii) ohmic insulation, i.e. find all possible shorts between neighboring channels. The work with a prototype chamber allowed us to identify the main error types in the pixel boards and to develop methods to repair them. Based on that experience, a three step test procedure was worked out.

The first test searched for connections between neighboring pads due to mistakes in the board production. It used a small test device consisting of an insulator board on which a number of spring-loaded test pins are mounted in a specific two dimensional pattern fitting the pixel geometry. A part of a pixel board together with the pin pattern is shown in Fig. 7. The spring loaded test pins (INGUN GKS-422-0123) with round heads made a reliable contact without destroying the fragile 5 μm copper layer of the pads.

The pins were set at different voltages in the range of 1–5 V. A simple electronic circuit checked the contact between pins. In order to scan the board quickly and efficiently, the contact pins and the electronic unit are attached to an *x*–*y* positioning system.

The pad in black in Fig. 7, could potentially have been shorted to any of its six neighbors shown in grey in the panel “Step 0”. During the test, the pattern of pins was moved through the pad structure in steps, each step corresponding to a pad column. In “Step 1” only one pin touched the black pad, and the hatched pads were tested against shorts to the black pad. By moving the pin pattern further, all neighboring pads (“Steps 2 and 3”) were checked.

The microconnectors were then soldered and the Kapton cables were inserted. As the second test, the soldering and cables were checked for shorts between neighboring leads. Legs corresponding to neighboring electrical lines are on opposite sides of the connector. Thus, every second trace could be contacted by shorting all the traces on one side of the microconnector with a conductive rubber. Using a probe pin, connected to a beeper every other lead in the connector and cable was then checked for shorts to its neighbors.

The final test controlled the continuity of the whole chain. The pixel board was placed with pixel side up, and the open end of all Kapton cables were shorted to ground on the opposite side of the board. A pattern of pins connect to the outmost

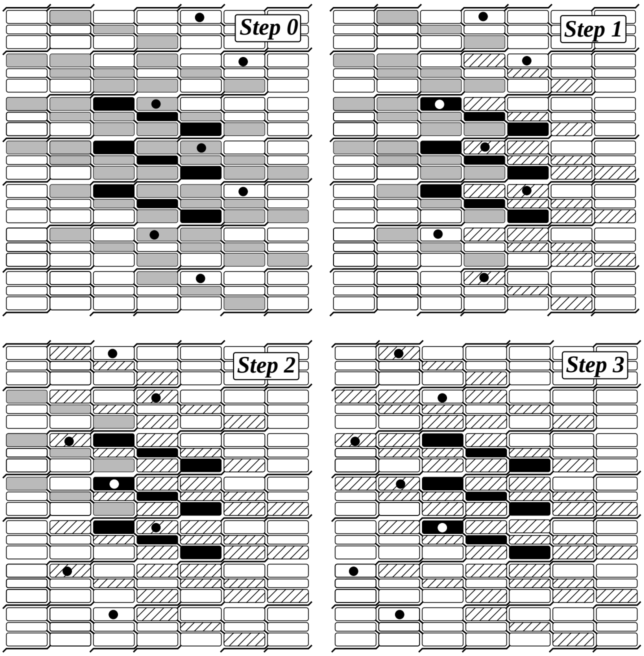

Fig. 7. The pad structure together with the pattern of test pin positions (circles) used in the first test. An arbitrary chosen pad is shown in black with its six neighbors in grey (Step 0). The pins are moved from right to left in steps of one column. Neighboring pads checked in each step (1–3) are hatched.

pixel in each pad in a way similar to what was done in the first test and the connection to the grounded far end of the Kapton cable was verified.

4.3. Chamber construction

The first step in the chamber production was the soldering of the microconnectors. A procedure based on surface mount techniques was developed which allowed very high soldering quality, minimum amount of soldering material as well as speeding up the soldering process. The solder paste was applied at the soldering places through a 0.2 mm thick stainless steel mask. The connectors were then installed in place and the joints were heated with hot air.

After soldering the microconnectors, the pixel board was tested using the procedure described above and repaired if needed. The sandwiches consisting of the honeycomb between two fiberglass boards were then glued together. The circuit board material, used in the construction, is one-sided copper-clad FR-4 fiberglass boards for the solid cathode and double-sided copper-clad board for the pixel board and motherboard, whereas the fourth board has no copper cladding. Gluing was done on a flat granite table using a vacuum bag pressing the pieces together. Special care was taken to minimize the amount of epoxy used for the gluing of the large surfaces. An average epoxy layer thickness of approximately 50 μm was used, controlled by weighing the amount of glue prepared before and remaining after the operation.

Each one of the ~4500 plated-through holes in the pixel board must be filled by epoxy for gas tightness. Every PC1 panel was checked for its deformation due to gravity and due to intrinsic tensions in the structure of the panels. Cathode and pixel panels with similar intrinsic deformations were selected in pairs in order to allow the deformations to compensate each other.

Before the assembly of the anode wire plane, the terminal boards were equipped with the electronics components and tested for HV. Terminal boards and wire support were glued to the pixel panels. The PC1 wire planes with the two types of wires were prepared on a winding machine in advance and moved to the detector using transfer frames. The wires, aligned to the pixel pattern using optical systems, were glued to the terminal boards and then soldered. A simplifying construction feature of the pixel readout system is its moderate demand on alignment between the wires and the etched pixel pattern. The measured alignment between wires and pixels is always better than 100 μm, well within the requirements.

Before the permanent glue sealing of PC1, a preliminary test was performed to verify the chamber functionality. The chamber was closed in a gas box filled with P10. After demonstrating clear anode signals from cosmic rays in all four HV-sectors, the chamber was permanently sealed. After sealing, deformation and gas leak rates were measured. The total leak rate of all 16 PC1 chambers was less than 1 ml per min. The chamber, suspended at the four corners showed typically less than 1 mm sag due to its own weight. Intrinsic deformations were substantially smaller than that. Tests showed that even a 3 mm deformation does not significantly affect the chamber performance due to the robustness of the pixel readout concept.

In order to build a pixel panel for PC2/3, two pixel boards with microconnectors were placed face down on a tooling plate. The two pixel boards were joined by gluing to the S2-glass frame and the S2 joint tube. The honeycomb was glued to the back of the pixel boards (inside the frames). Finally the motherboard was added. The entire panel was placed under vacuum until the epoxy had cured. The plain panels were constructed similarly, except that there were no Kapton cables and the plain copper surface was placed next to the flat surface.

On the PC2/3 pixel panel the wire terminal boards were glued to the pixel panel and the wires were strung onto the panel, placed on a rotating winding table. The wires were fixed by epoxy at both ends before cutting them to allow the wound panel to be removed from the winding table. After soldering the wires to the traces on the terminal boards, S2 bars, housing the O-ring were glued around the edge of the gas volume. As the final assembly step, the plain panel was bolted together with the pixel panel and the chamber could be tested for gas tightness and HV performance. Typically, leak rates of a few ml per minute were obtained for PC2/3.

Finally the connector cards (cf. Section 5) were soldered on the motherboards (~2500 contacts per chamber) using the same surface mount technique which was developed for soldering the microconnectors. Other details permanently mounted on the motherboard are pin headers for the flat cable connections from the motherboard and termination resistors at the far end of the communication busses.

When the ROCs had been connected to the connector card and the Kapton cables, the chamber was ready for the cosmic test which was the final stage before mounting the chambers on the spectrometer carriage. Typical results of the cosmic tests are reported in Section 6.

4.4. PC1 chamber mounting

The PC1 chambers were mounted directly onto the back of the DC (Fig. 8). No mounting material is placed in the active region. Mounting brackets with a cylindrical rod extend out from each of the four corners of a chamber. These rods attach to four couplers which stand off the outer radius of the DC. The couplers allow position adjustments in all directions. Survey marks on each PC1 chamber allow the chambers positions to be determined relative to survey targets on the DC. This is crucial because there is no point on PC1 that can be viewed once it is installed and all

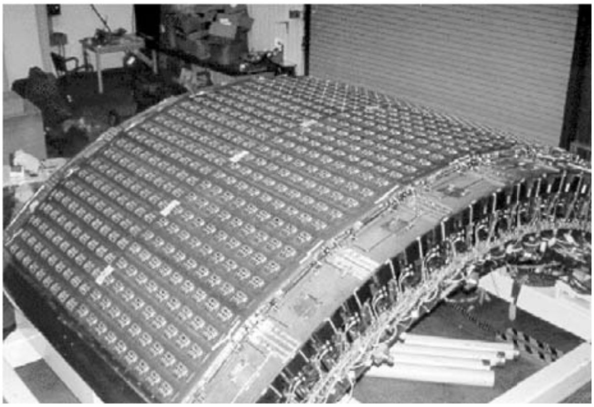

Fig. 8. PC1 chambers mounted on a drift chamber.

position information must be related to secondary targets.

DC and PC1 can be separated electrically from each other, but experience showed that the best common performance was achieved if the DC (being most sensitive) and PC1 were grounded together. The PC1 chambers have the ROCs on the outer surface, away from the DC due to safety and noise considerations. A flame-proof vinyl window protects the RICH in case of a component failure causing overheating on a ROC.

4.5. PC2/3 chamber mounting

Two PC3 (or PC2) chambers were mounted together to form a 22.5° sector, separated at the $z = 0$ plane. The two chambers were held together with an H-frame construction using an aluminum I-beam. The H-frame does not extend into the active area of the chambers as it covers only the chamber frames. The H-frame serves like a pair of rails, allowing the PC2/3 chambers to be slid into the frame. The H-frame is held together at $z = 0$ by a pair of stainless steel threaded rods which keep the two rails from separating in the center. At the outer edge, the H-frame is bolted directly to the PC3 chamber. This gives the H-frame rigidity. The entire package of two PC3 chambers in their H-frame were mounted on the outer surface of a TEC sector. The H-frame is bolted to the TEC at each of the four corners, and at the middle of the two rails. This keeps the inner surface of the PC3 chambers spaced a uniform 2.5 mm away from the TEC frame. The PC3 chambers also serve to keep the thin TEC window from ballooning out because the window is pressed up against the PC3 panel by the slight gas overpressure in the TEC.

PC3 is mounted with the ROCs facing away from the TEC for safety and noise reasons. The TEC and PC3 can be operated isolated from each other but the best common noise performance has been achieved by grounding them together. The EMCal situated next to the ROCs has been shown to be insensitive to possible digital noise from PC3.

In the west arm, both PC2 and PC3 are present but there is no TEC, an aluminum box construction constitutes a mockup for the TEC and provides a structure for PC mounting.

Like PC1, there are survey marks on the PC3 chambers which allow the PC3 positions to be determined relative to survey marks on the TEC. No survey of the PC3 chambers is possible after it has been installed on the east arm.

5. The readout electronics

A unique property of the electronics for the Pad Chamber system is that a substantial part of it is mounted on the chamber planes in the path of the particles. A minimal amount of material in the electronics circuits was therefore a major design goal. Since it was to be built in several hundred thousand channels, it was necessary to incorporate all functions in two new Application Specific Integrated Circuits (ASICs) named TGLD and DMU. These are mounted on ultra thin readout cards (ROCs), the part of the front end electronics mounted in the fiducial volume.

On the detector, but outside the fiducial volume, the FEM circuit (Front End Module) handles the communication and power distribution to the ROCs, collects the data from the ROCs and formats the data for transport off the detector. Global timing synchronization is provided by the Timing and Control system (T&C) as well as trigger requests and other fast instructions which may change from one cycle to another. Together, the ROCs and the FEM constitute the Front End Electronics (FEE). The FEM communicates via fiber optics with the data collection module (DCM) and the T&C-system in the counting house. Programmable configuration control of the FEM and the TGLD chip is provided by a slow control line using the ARCNet protocol. The block scheme in Fig. 9 illustrates the architecture of the readout system. In this section we describe the function of the readout electronics and its performance.

5.1. *The charge sensitive amplifier/discriminator chip, TGLD*

An electronics channel for the Pad Chamber detector compares the amplified input signal with a threshold. The block diagram in Fig. 10 illustrates the main components in one channel of the amplifier/discriminator chip [11]. Each channel consists of a charge sensitive preamplifier (CSA), a voltage amplifier, a test pulse generator, a CR differentiator, a leading edge (LE) threshold discriminator, a one-shot generator and a voltage to current output stage. The design sensitivity of the readout system was determined by the requirements imposed by PC1 which has the

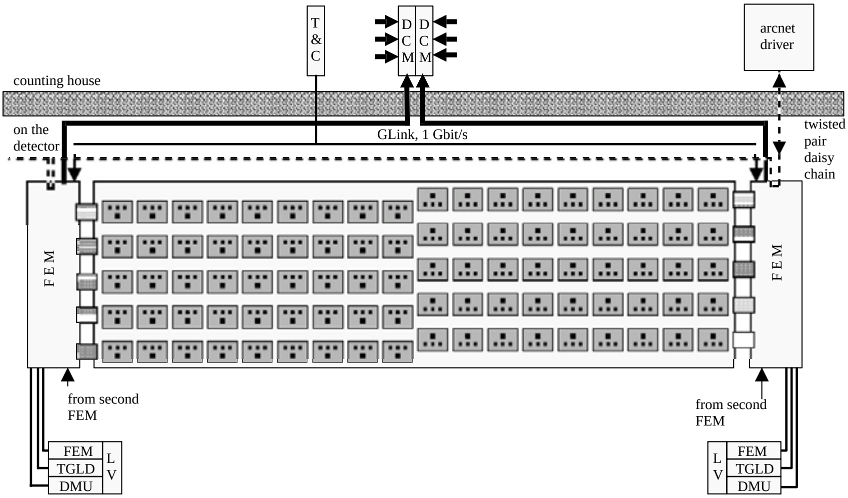

Fig. 9. Full system architecture, handling 4320 channels on a PC1 chamber.

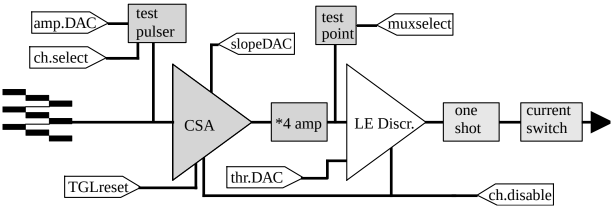

Fig. 10. Block scheme of a single channel.

thinnest gas gap. The most probable signal on a pad is 18 fC corresponding to the most probable anode charge at the nominal gain setting (50 000). In order to obtain full plateau efficiency one should be able to set the threshold at 10% of the most probable charge, i.e. about 2 fC.

The CSA has a charge to voltage conversion gain of 2.5 mV/fC and an adjustable time for return to baseline. For reliable restoring of the baseline after saturation, the preamplifier needs to be reset on a 100 Hz basis. A voltage amplifier provides further amplification by a factor 4 resulting in an overall sensitivity of the amplifier stage of 10 mV/fC. The AC coupled, input signal to the discriminator can be attenuated by a factor 3 or a factor 9 for a larger dynamic range. For normal operation, the setting with no attenuation is used, giving a threshold interval of 1.5 to 10 fC with ±0.25 fC maximum channel to channel variation. The one-shot ensures that the current output is always a 75 μA, 150 ns wide pulse. A reference output current of 25 μA (common to all 16 channels in a chip) defines the on/off switching level for safe interpretation of the signal levels by the receiver stage of the DMU. Current mode is preferred to voltage mode for these digital signals as it gives robustness against crosstalk and common-mode pickup noise.

The simulated value of the preamplifier noise corresponds to 590 electrons at 0 pF input capacitance with an additional 32 electrons per picofarad of pad input capacitance (23 pF for PC1, 36 pF for PC2, 43 pF for PC3). This noise is a factor 5 lower than the minimum settable discriminator threshold. Oscilloscope studies have qualitatively verified these noise values by observing the test point after the voltage amplifier, where the analog signal of a selected channel can be connected to an output pin by an analog multiplexer. The test pulse generator can inject a selectable test charge (0–127 fC) at the preamplifier input.

Each chip has 16 parallel channels. The discriminators have a common threshold. Careful control of low voltage distribution and decoupling among the three main stages was needed to avoid crosstalk between channels at the lowest thresholds. Many functional characteristics can be controlled remotely, through a serial communication where each TGLD has its own 5-bit address. The most important programmable features are the on-chip digital to analog converters by which thresholds and test pulse amplitudes are set. Individual channels can be disabled as well as selected for test pulsing. Downloaded serial control information can be read back for consistency check.

The preamplifier reset is in itself a source of noise, internally in the chip as well as over the full system, due to induced charge from the reset switching. The internal reset sequence was carefully timed, in order to minimize these effects and in addition, the discriminator function was gated off, thus avoiding simultaneous firing of all discriminator channels in the system in conjunction with the reset.

No special attention needs to be paid to radiation hardness. This CMOS chip, designed for the 1.2 μm CMOS process at Orbit semiconductor (now Supertex), has an area of 3.7 × 3.7 mm^2. The power consumption is in total about 50 mW, i.e. about 3 mW per channel.

5.2. The digital memory and derandomizer unit, DMU

The main functions of the digital memory unit, DMU (Fig. 11), are:

- To sample the discriminator output signals from three TGLD chips (48 channels) for each clock pulse (RHIC beam crossing).
- To store all data until the first level trigger arrives.
- In case the first level trigger arrives, to provide storage of the corresponding event until readout is completed.
- To provide storage of at most five events, to accommodate the random occurrence of events.

Filling of data into the DMU is driven by the clock while emptying of events is controlled by the readiness of the readout chain. The clock frequency, equal to the beam crossing frequency of RHIC, is 9.38 MHz (the circuit is operational up to 40 MHz).

The communication between TGLD and DMU is specially designed to minimize the noise generated by this digital activity. When a TGLD output is in a TRUE state (channel fired), it delivers a 75 μA current (equivalent DC current). This is sensed as TRUE by the input circuit of the DMU if the current is larger than a reference current (25 μA) also provided by the TGLD chip. By this automatic signal normalization we obtain transfer reliability, in spite of the extremely low signal levels.

The delay memory stores data for each beam crossing until a possible receipt of a first level trigger. The memory is 48 bits wide (one for each channel) and the depth address (i.e. what beam crossing the data belongs to) is determined by the beam clock counter. The memory is a dual arrangement where writing and reading is performed in an alternating sequence between the two. Reading and writing can be done in the same cycle, however in opposite banks. The total depth until data is overwritten is 44 clock cycles, determined by the time it takes to produce the first level trigger in PHENIX. The depth is selectable up to the hardware limit (64) by a

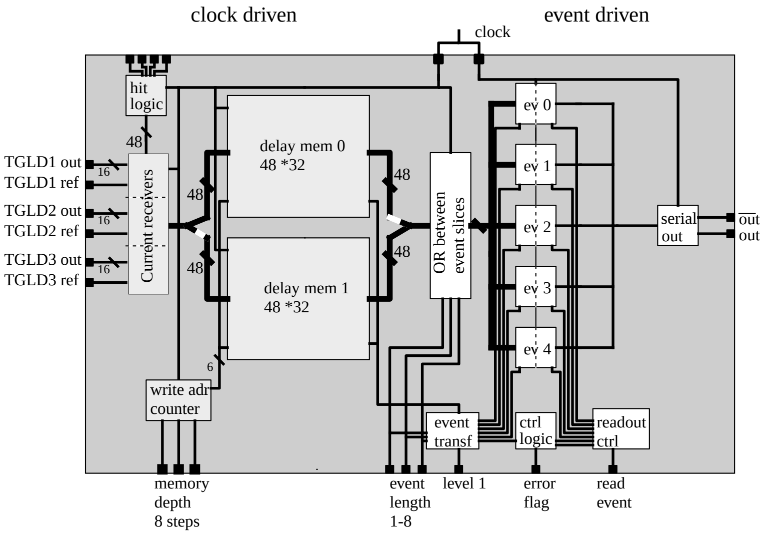

Fig. 11. Block scheme of the DMU chip.

three-bit binary code, strapped via external pins at the time of ROC assembly.

If a trigger arrives, the data fed into the DMU 44 clock ticks earlier is moved from the delay memory to one of five event memories. Data belonging to the same collision can be spread out in time by several hundred nanoseconds due to: flight time of the particles, drift time in the wire chambers and timing walk in the leading edge discriminator. Collecting the data in four time slices (the number of slices is selectable by strapping) is sufficient to catch all data belonging to an event. It is not worthwhile to keep the information which of the four time slices the bit belongs to. Thus a bitwise OR is made between the four slices before data is stored in the event memory.

Upon receipt of a READ_EVENT signal, data is read from the event memory. Data is sent serially as complementary CMOS signals thus allowing reliable transfer over the long distances to the FEM (2 m on PC3). The address of the event memory, accounts for the first three bits, followed by the 48 data bits and a trailing parity bit as a final check of the data transfer.

The DMU chip was designed[12] for the 1 μm CMOS process at AMS (Austria Mikro Systeme Int.).

5.3. The readout card and the connector card

The large number of channels per unit area, a major merit of this detector, made it necessary to mount the part of the electronics where all channels are treated in parallel i.e. up to the DMU output, on the backplane of the wire chamber. A problem to solve in this context was to reduce the amount of material in the electronics in order to minimize the effects of secondary interactions by particles passing through. A potential difficulty would also be the presence of digital signals close to the highly sensitive charge inputs. On the other hand, a short distance from pad to preamplifier is an advantage from a noise point of view.

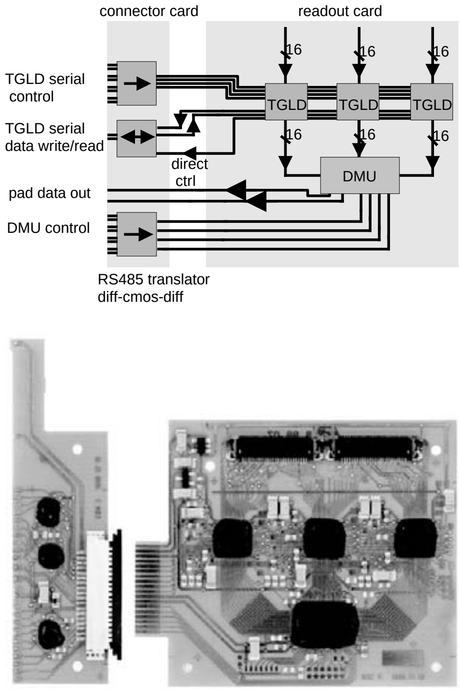

Fig. 12. Block scheme of the connector and readout cards and a photograph showing how they look in reality. The ROC area is 20 cm^2.

Fig. 12 shows the block diagram of the circuits on the readout card (ROC) and the connector card. A ROC receives the input signals from 48 pads via two flexible Kapton cables and distributes them to the three TGLD chips. The discriminator results are transferred in parallel and stored in the DMU.

The chips on the connector card translate the differential control signals bussed through a row of nine ROCs to a single ended CMOS signal standard. The well defined functions on the connector card are obtained by commercially available chips. It was convenient, both from development and manufacturing point of view to separate this part of the design from the more critical, custom made chips placed on the ROC.

---

[12] The DMU chip was developed by SiCon AB, Linköping, Sweden.

The TGLD and DMU chips on the readout card and the translator chips on the connector card are mounted with the chip-on-board technique on fiberglass reinforced polyimid circuit boards of 100 μm thickness[13]. In this assembly technique, the naked silicon dice are glued to the circuit board and the electrical connections are done by ultrasonic wire bonding from the connector pad on the silicon, directly to the circuit board. Besides the minimal amount of material, this technique has advantages of low cost and excellent signal performance due to the extremely short connections. Passive components are surface mounted with conductive epoxy. After functional test, the chips are covered by a glob of hard epoxy, which protects the chip and the bondwires mechanically and stiffens the flexible card in the bonding area. The black epoxy also protects the chip from ambient light. An option, to cover the glob by conductive (grounded) paint for RF-shielding, proved to be unnecessary.

The connector card was soldered onto traces on the motherboard, which is the outer fiberglass board of the cathode sandwich. The ROC can easily be dismounted since it plugs into a 1 mm pitch Flexible Printed Circuit (FPC) connector on the connector card. The Kapton cables from the pads connect to FPC connectors (0.5 mm pitch) on the ROC.

Together, the connector card and the ROC (including the Kapton cables and connectors for pad connection) weigh 4.8 g. On PC1, where the density of ROCs is one per 100 cm^2, this amounts to 0.2% of a radiation length when averaged out over the detector surface. On PC3 the corresponding value is 0.05% due to the factor 4 lower ROC density.

5.4. The motherboard and the system noise

The upper fiberglass board of the cathode panel is also the electronics motherboard where all signals and DC-voltages are distributed from the FEM at the side of the detector to the ROCs and output data is sent from the ROCs to the FEM. The opposite side of the motherboard is a continuous ground plane, to which the analog ground of each ROC is tied locally. This ground plane provides an efficient shielding of the noise sensitive pads from the continuous digital activity on the motherboard traces and in the DMU. In order to reduce the noise generated by digital signals on the motherboard, these are distributed as differential RS485 standard, with which we achieve reliable communication over long distances (about 2 m on PC3), even using as low signal amplitudes as 0.7 V. As a compromise with timing accuracy, amplitudes of 1.4 V are used.

The DC-supply to the analog and digital chips on the ROCs suffer from the long distances and thin copper on the motherboard, although these traces were made extra wide. Thus the ROCs are equipped with low dropout voltage regulators for the TGLD power while the DMU is tolerant enough to accept the variation in supply voltage over the length of the trace.

During regular data taking the thresholds are set at 5.4 fC for PC1 and 7.2 fC for PC2/3. With these thresholds, no channel ever fired either on random noise or on pickup noise from the digital activity. The lowest common threshold for the whole system that was usable, with totally noise free operation, was 2.5 fC for PC1 and slightly higher on PC2/3.

5.5. The FEM and the data transfer to the DCM

The Front End Module (FEM) [12] is placed at the side of the detector and connects to the motherboard via short flat ribbon cables, one for each ROC row. Each FEM handles the control and data collection from five rows of nine ROCs each (Figs. 9, 13), i.e. 2160 channels. On PC1 there is one FEM card at each end of the chamber, while PC2 and PC3 have two FEMs on the same side of each chamber.

The FEM card has a programmable readout and control module (called the heap manager), implemented in a Xilinx 4020 field-programmable gate array (FPGA). This provides control signals to the ROCs, collects and transmits data, and manages the command interface (timing and control). A second FPGA of the same type

---

[13] The chip on board assembly on thin flexible boards was developed by XICON AB, Malmö, Sweden.

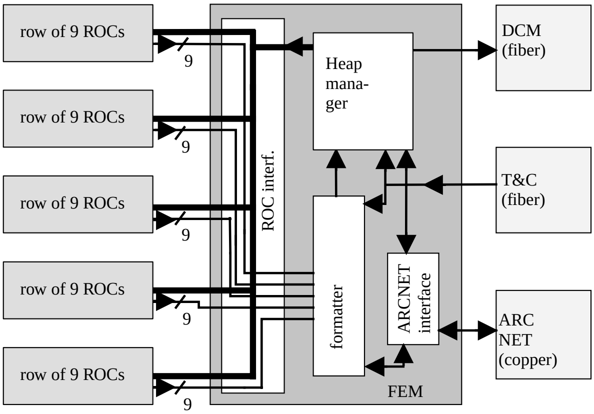

Fig. 13. Block scheme of the Front End Module (FEM) card.

controls the serial data readout from each DMU and serial-to-parallel data conversion. Additionally, an embedded controller is included for transmission of slow serial data and control information to the FEM and the ROCs via ARCNet protocol. Fig. 13 shows the generalized architecture and the data flow path associated with the FEM and its interfaces.

The signal interface to an individual ROC row includes separate voltage regulators for TGLD power, DMU power and RS485 chip power (signals to DMU only). All signals from the FEM to a ROC row are sent by RS485 transmitter chips. Receiving of data from ROCs is done by RS485 receiver chips on the FEM.

Each FEM receives system clocks and mode control signals directly from PHENIX Timing and Control (T&C) via a GLink fiber at 37.5 MHz, i.e. four times the beam clock frequency. Serial data from each DMU is clocked out to the FEM, all 45 in parallel. Data is converted into 20-bit words by the data formatter for transmission by the heap manager over the GLink fiber. The data format reflects the pad location such that a 20-bit word contains the result from 20 pads across five ROC rows on the chamber. Twelve such words contain the data from five ROCs, one from each row. A full event produces 108 (9×12) such 20-bit words per FEM, and this data block is a direct image of the pattern of hit pads on the chamber with the bit position in a word being the location across the wires (ϕ) while the word number is the position along the wires (z-direction). This format is useful for later data handling and analysis speed.

The ARCNet interface provides slow serial communication to the front end electronics from the high level control of PHENIX. Its functions include programming of the FPGAs after a cold start or hard system reset, loading of the ROC/TGLD control bits (channel enables, threshold settings, calibration enables, multiplexer controls), resetting the GLink interfaces, and controlling the heap manager self-test function. Readback capability exists at every level allowing readback of FPGA 'done' condition, GLink synchronization status, and complete readback of heap manager and ROC/TGLD programmable parameters.

The FEM also includes a built in self-test (BIST) function which produces a set of known packets. Use of BIST mode helps certify FEM operation independently of the ROCs' status.

The data collection module (DCM) receives the data through the 1 Gbit/s GLink. Together with the data words, a few words at the beginning are reserved for event header, event number, clock counter, FEM address etc. At the end of the buffer additional words like parity check of the FEM-DCM communication are found. The 20-bit result words are restored in the DCM and here zero suppression can be done. A simple zero suppression, just skipping 20-bit words which are zero, gives an average reduction to four 20-bit words per particle hit. The DCMs are read out to the event builder, together with DCMs for other Pad Chamber FEMs and other PHENIX detectors, where the data is assembled into full events which are sent to archiving and software analysis.

5.6. FEM mounting and cabling

The FEM cards are housed in aluminum boxes which are fixed to the chambers. The boxes provide electrical shielding and an additional safety barrier against overheated components. Five short, 50 conductor ribbon cables bring the ROC signals out from the motherboard to each FEM where they enter the aluminum FEM housing through narrow slits.

Optical fibers are used to bring timing signals to the FEMs and data from the FEMs. The FEMs are read out in duplex mode, with one FEM passing its data along to the other FEM which communicates with the DCM. Each FEM requires a timing signal brought in on a fiber, while a readout fiber is only needed on the first FEM of a pair. Data transfer from the second to the first FEM goes via a pair of RG174 coaxial cables, using the GLink protocol at 800 Mbits/s.

In addition each FEM only requires one low voltage cable (with 3 pairs of power and ground in each) and the daisy chained twisted pair ARCNet cable.

6. Performance of the Pad Chambers

Each fully instrumented Pad Chamber was tested with cosmic rays before installation. The purpose of the test was to verify the gas gain at running conditions i.e. an argon–ethane 1:1 mixture at atmospheric pressure. By sensing the produced charge at the wire, the signal connection from each pixel to the input of the preamplifier was reconfirmed. The operation of the electronics alone was also tested by the internal test pulse in the TGLD chip and the self test of the FEM.

One chamber each of PC1, PC2 and PC3 was extensively tested with cosmics for efficiency calibration and determination of the position resolution (only PC1 and PC2). Fig. 14 shows the setup used for the cosmic measurements. Two large area plastic scintillator planes (SL1, SL2) of approximately the size of a PC1 chamber, were placed above and below the chamber under study. The chamber was placed on a thick granite table, acting as an absorber of low energy particles. Each scintillator plane consisted of five scintillator bars, read out at both ends by photomultiplier tubes. A triggering particle required coincidence between the two photomultipliers of a scintillator bar. A

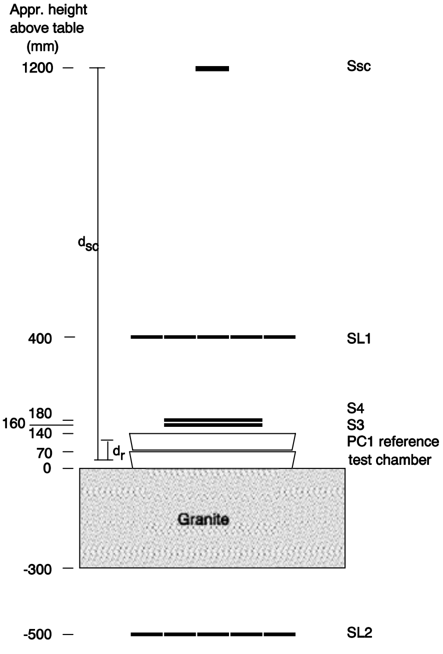

Triggers:
Chamber mapping: SL1 & SL2
Efficiency measurement: SL1 & SL2 & S3 & S4
Position resolution meas. :SL1 & SL2 & Ssc

Fig. 14. The cosmic trigger arrangement.

coincidence between a hit scintillator bar in each layer constituted a cosmic trigger with about 1% random coincidence rate.

For the efficiency measurements, an additional scintillator (S3) of size $33 \times 58\ \mathrm{cm}^2$, was placed right on top of the chamber under study, thus defining a large area but still well within the sensitive area of the chamber. Cherenkov light, produced in the lightguide between the scintillator and the photomultiplier, produced triggers outside the well defined area and thus a fourth scintillator (S4, identical to S3) was placed right on top of the third scintillator but oriented with the lightguide in the opposite direction, thus avoiding hits in the lightguides to trigger the system. This four-fold coincidence provided a cosmic trigger with negligible random rate. It was used in all measurements described below, except for the studies of the position resolution.

6.1. The charge gain on the anode wires

The anode wires of the Pad Chambers had no wire readout installed, but for a few wires of each chamber type, the wire signal was extracted over a capacitor to an ORTEC 142B preamplifier followed by a spectroscopy amplifier system. The pulse height distribution was recorded on a LeCroy QVT multichannel analyzer, and the peak of the pulse height distribution (representing the most probable energy loss by a minimum ionizing particle) was determined. Fig. 15 summarizes the anode charge measurements for different high voltage settings for the three chamber types. The measured charge, relies on the absolute calibration of the spectroscopy amplifier readout chain. The absolute uncertainties due to the calibration and due to the determination of the peak position of the Landau distribution, add up to ±25%.

The charge gain was determined by dividing the charge corresponding to the peak with the most probable initial ionization by a minimum ionizing particle. This was calculated to be 95 electrons per cm for this gas mixture using tabulated values for the average energy needed to liberate an electron ion pair in argon and ethane. The average for the two gases is 26.4 eV. The energy loss for the gas mixture was weighted by the elemental composition of the gas [13]. This calculation reveals the average number of initial electrons. Since the quantity measured is the most probable (peak position) charge, the value was modified to the most probable value of the Landau distribution.

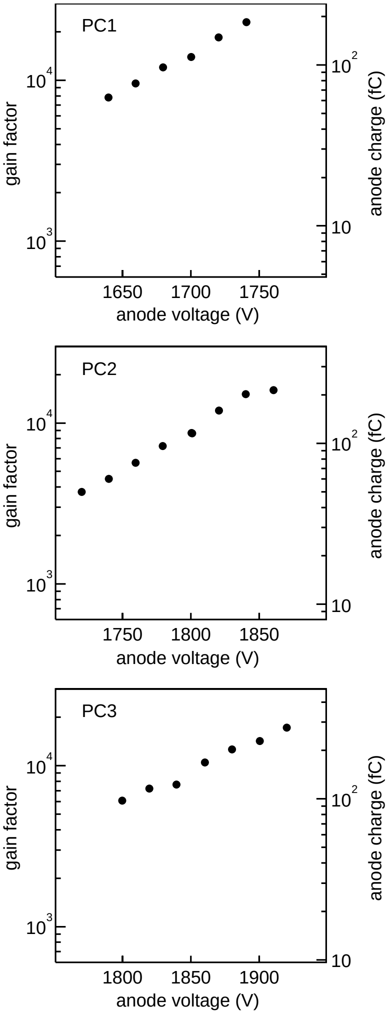

Fig. 15. Gain curves for PC1/2/3.

The HV-ranges used are safely below the onset of sparking and all chambers built are operational at gains up to at least 50 000.

6.2. *Efficiency measurements*

The chamber efficiency was studied as a function of high voltage and threshold setting. The cosmic trigger in the four-fold coincidence mode was used. The area defined by the trigger involves fifteen ROCs on PC1 and eight on PC3. The area selected for the studies was typical for the performance in those parts of the detector which were unaffected by the central wire support. The charge gain was recorded for each efficiency measurement for gain normalization.

In addition to the efficiency, these measurements reveal the cluster size distribution, i.e. the number of pads and cells fired for each detected particle. On the level of 5%, a trigger particle is accompanied by another particle hitting the chamber. This second particle must coincide with the trigger particle in a window of about 400 ns in order to be detected in the chamber. Its origin is therefore most probably the same cosmic air shower as the trigger particle. Such events were omitted from the analysis if the two hits were easily distinguishable. Only if the distance between the two hits was less than 3 cm was there a risk not to be able to recognize them as two. Less than 0.1% of the events are estimated to be unresolved double hits.

Fig. 16 shows the number of pads for which the discriminator has fired, at different high voltage settings on the anode wires. The threshold setting for all studies except when the threshold is the varying parameter corresponds to 5.4 fC collected charge on the cathode pad for PC1 and 7.2 fC for PC2/3. These thresholds are the same as those used during real data taking and it never happens that a channel fired due to electronics or pickup noise. We show only the result for PC1 but very similar results were obtained for PC2/3 at corresponding high voltage settings.

When the chamber gain is too low (HV below 1700 V) a fraction of the events have no pads fired. At 1680 V, it never happens that only one pad

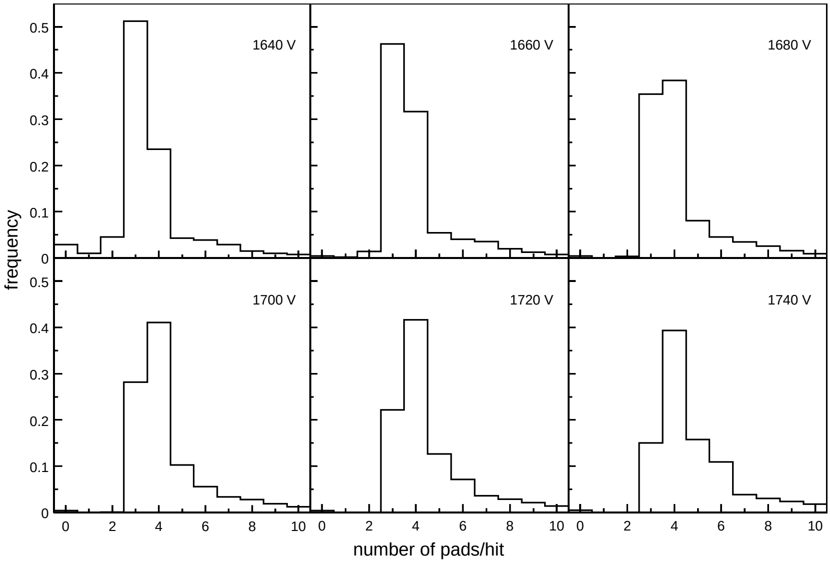

Fig. 16. Pad multiplicity distributions for PC1.

fired while it does happen that only two pads fire when the voltage is too low. At 1700 V and higher, the fraction of two pad events is also negligible. The fraction of completely empty events levels out at the higher voltages, indicating that a plateau efficiency has been reached. This small fraction (less than 0.5%) is interpreted as a real inefficiency as it cannot be reduced by further gain increase.

For Fig. 17 the results have been transformed from pad space to cell space, i.e. all cells for which the three neighboring pads have fired have been labelled as fired cells. The number of fired cells per hit is displayed. The fraction of events with no cell fired is exactly the sum of no-pad and two-pad events in Fig. 16. Our basic criterion of a detected particle is that at least one cell must have fired. At 1700 V and higher the fraction of events with no reconstructed cell is very small and basically constant. It is also noticeable that the fraction of one cell clusters compared to two-cell clusters depends sensitively on the high voltage, indicating that it can be used for efficiency monitoring. It is also clear that three fired cells is a rather unlikely situation as expected from symmetry arguments, while four cells (two by two) is more probable.

The results for PC2 and PC3, corresponding to Figs. 16 and 17, are quite comparable to the PC1 results.

The efficiency is calculated as the number of events producing at least one fired cell divided by the number of cosmic events as defined by the 4-fold coincidence in the cosmic setup (Fig. 14). In Fig. 18 we summarize the efficiency information as a function of high voltage for the three chamber types. Clearly a plateau efficiency is reached for all chambers. The plateau is 99.6% for PC1 and 99.8% for PC2 and PC3.

The filled circles represent the basic "fired cell" definition, i.e. three adjacent pads fired. The open squares are obtained if also two adjacent pads fired are accepted as a valid hit. The plateau efficiency is then reached at a lower (by about 20 V) voltage. The probability that two neighboring pads could fire on noise is negligible and one could operate the system at somewhat lower sensitivity if one accepts two fired neighbor pads as a fired cell for the

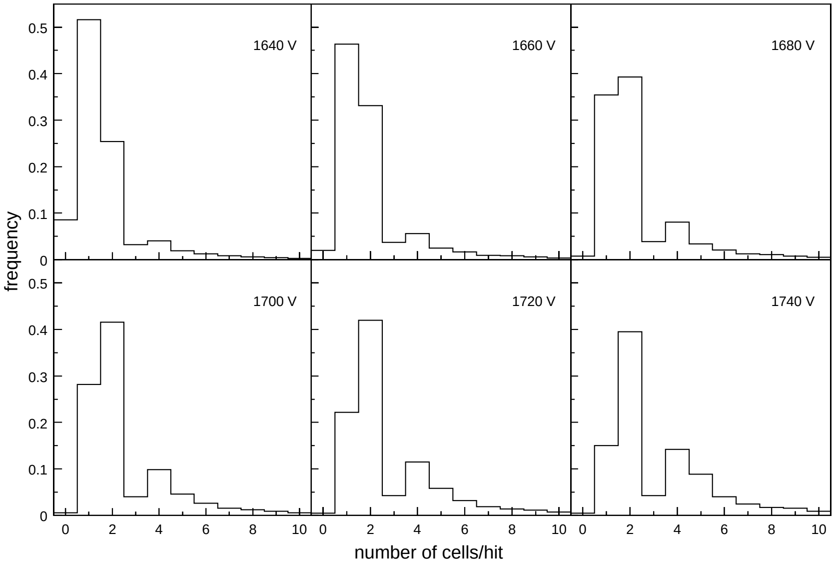

Fig. 17. Cell multiplicity distributions for PC1.

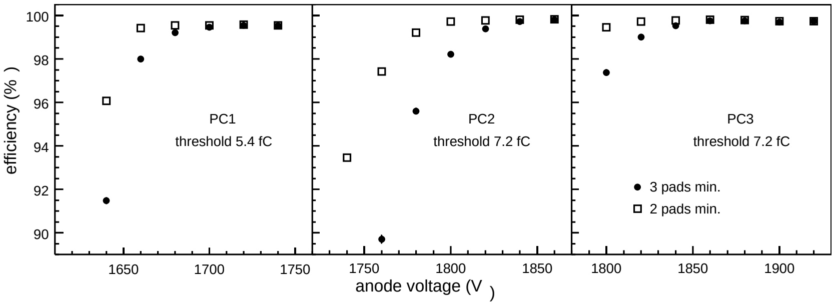

Fig. 18. Efficiency curves for PC1/2/3 with varying high voltage at the operation thresholds.

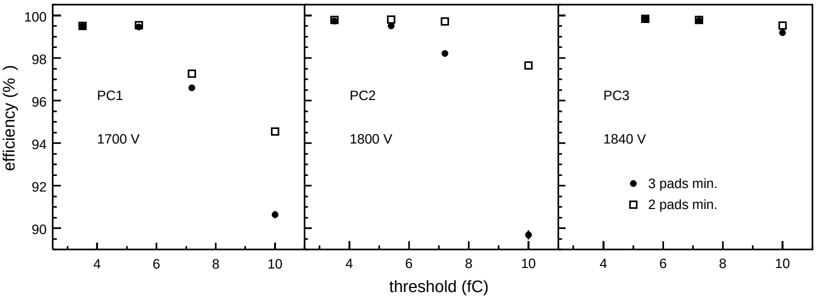

Fig. 19. Efficiency curves for PC1/2/3 with varying threshold at the operation HV.

weakest avalanches. This would result in reduced cluster sizes which is beneficial for operation at high multiplicity.

In Fig. 19 the HV was kept constant and the discriminator thresholds were instead varied from 3.5 to 10 fC. The lowest threshold was completely noise-free for PC1 and PC2 while on PC3 the lowest, noise-free threshold was 5 fC (limited by coherent noise on a few pads). Changing the sensitivity by adjusting the threshold is equivalent to changing the gain of the chamber as long as the thresholds are well above the noise level.

As a summary of the efficiency studies we use as a sensitivity parameter, the normalized threshold expressed as its fraction of the anode charge [14] at the peak as can be seen in Fig. 15. If the pad geometry as seen from the wire (i.e. the charge pickup properties) are the same for the three

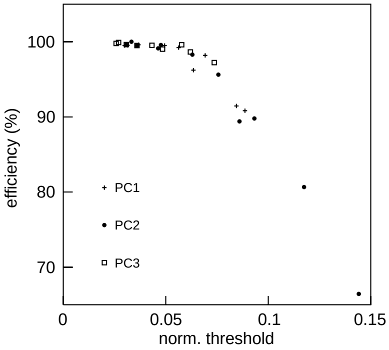

Fig. 20. Efficiency vs. threshold, normalized to the anode charge.

chamber types, all efficiency data should fall on a unique curve when displayed versus the normalized threshold. This is clearly the case as displayed in Fig. 20, where the efficiency data for all settings of HV and threshold and all three chamber types are included.

6.3. *Efficiency monitoring*

Usually the gain in wire chambers is monitored by reading out the wire signals. In our case, this would require a complete parallel signal and data processing path with analog readout. Instead, we exploit the fact, already indicated, that the ratio between the fraction of two-cell and one-cell clusters in the cell multiplicity distribution in Fig. 17 varies sensitively, in a monotonic way with the efficiency. This variation is displayed in Fig. 21 showing that at a ratio of about 1 one would have optimal conditions. Monitoring this ratio for each chamber has sufficed to ensure the operation of the pad chamber system at plateau efficiency.

The ratio above can to some small extent be influenced by the angle of incidence of the particles. In particular the angles change depending on the magnetic field. Differences between magnet on and off were studied with the data from the first run. No noticeable effects were observed in the 2 cell to 1 cell ratio.

As an additional efficiency monitor we also studied the fraction of hits resulting in only two pads fired, which appeared in the pad multiplicity distribution in Fig. 16. These are due to hits located right between two cells along the wire. Here, two of the four pads involved collect only 50% as much charge, compared to the two pads that are members of both cells. This is the situation in which the weakest avalanches start to influence the efficiency. The ratio of three-pad hits to two-pad hits is basically governed by the pad geometry and provides an additional handle on the intrinsic chamber efficiency. As seen in Fig. 22, this ratio depends sensitively on the efficiency.

With these two complementary methods one can safely re-establish the calibrated operating point of the system, providing plateau efficiency at a minimal cluster size.

6.4. *Position resolution*

Minimal cluster sizes are required in order to obtain the best performance at high multiplicity as well as to achieve the best position resolution. Lacking a beam test, we have not been able to study the position resolution in the way one would like to, i.e. with beam and a reference chamber of better resolution. Since all aspects of the chamber performance studied so far have followed the simulations extremely well, one may expect that the position resolution should follow the simulated values as well.

We have performed a study of the position resolution using cosmic rays and two Pad Chambers placed, on top of each other in the cosmic test stand. One of the two chambers was used as the reference chamber and tracks were projected into

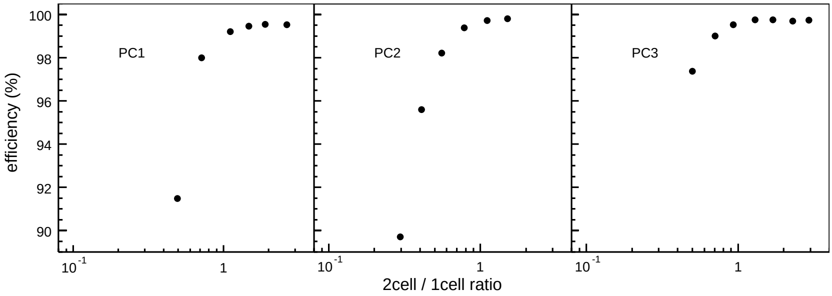

Fig. 21. Efficiency vs. two-cell/one-cell ratio.

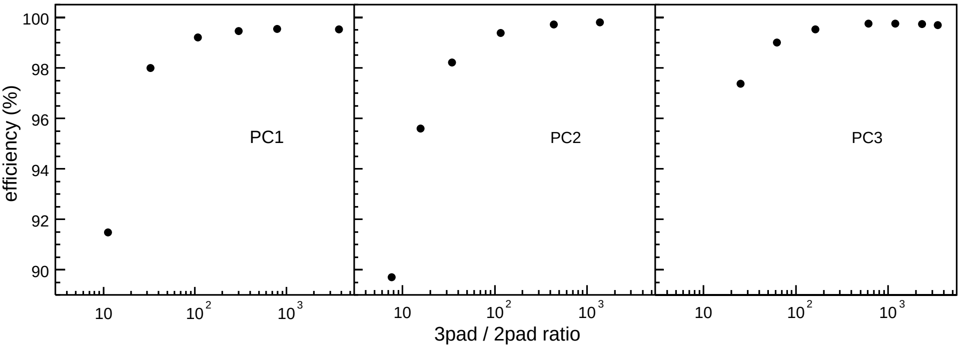

Fig. 22. Efficiency vs. three-pad/two-pad ratio.

the chamber under study by including a smaller scintillator placed at a distance of 1.2 m above the table (S_{sc} in Fig. 14). If the position resolution of the reference chamber is known as well as the position resolution of the small scintillator, one is able to calculate the position error (σ_e) in the track projection into the chamber studied. This error can then be subtracted from the measured position spread (σ_m) in this chamber to obtain the intrinsic (σ_i) chamber resolution.

$$\sigma_i^2 = \sigma_m^2 - \sigma_e^2$$

where σ_e is calculated from the inaccuracies of the scintillator and the reference chamber as

$$\sigma_e^2 = \left(\frac{d_r \sigma_{sc}}{d_{sc} - d_r}\right)^2 + \left(\frac{d_{sc} \sigma_r}{d_{sc} - d_r}\right)^2.$$

The distances $d_r = 70$ mm and $d_{sc} = 1165$ mm are indicated in Fig. 14. The position resolution of the small scintillator (σ_{sc}) is known since it is governed by its size. The resolution (σ_r) of the reference chamber is on the other hand unknown. But for the case where the reference chamber and the studied chamber are identical (in our case 2 PC1's) we have $\sigma_i = \sigma_r$ and we can solve the equations.

The procedure is as follows: First determine the position resolution of PC1, by using two PC1 chambers, one being the reference chamber. Once this is done we use the PC1 reference chamber also for determining the position resolution of PC2 and PC3.

Fig. 23 shows the result of the position resolution measurement along the wire for PC1 and PC2. The position resolution result along the wire (z-direction) is most straightforward to interpret as the measured distribution, i.e. the difference between projected hit position and the reconstructed position is a nice symmetric Gaussian. σ_m is obtained by fitting a Gaussian to the distribution and the intrinsic resolution in z (σ_i) is obtained from the formulae above.

The measured position resolutions (σ_i) along the wire are 1.7 mm in PC1 and 3.1 mm in PC2. This compares well with the simulated values 1.6 and 2.7 mm, respectively. One may expect that PC3 should relate to the simulations in a similar way with an actual position resolution slightly larger than the simulated 3.2 mm.

Across the wires one does not expect a Gaussian distribution but rather a rectangular one since positions can only be reconstructed to either wire. This is the case for tracks traversing perpendicular to the wire plane. Inclined tracks can however produce avalanches on two wires if traversing right between the two wires. In that case we could quite correctly reconstruct the hit to this middle position. Thus one can expect the measured distribution to be flat, with a rather sharp peak representing very accurately, the reconstructed positions, just at the field wire. These features are

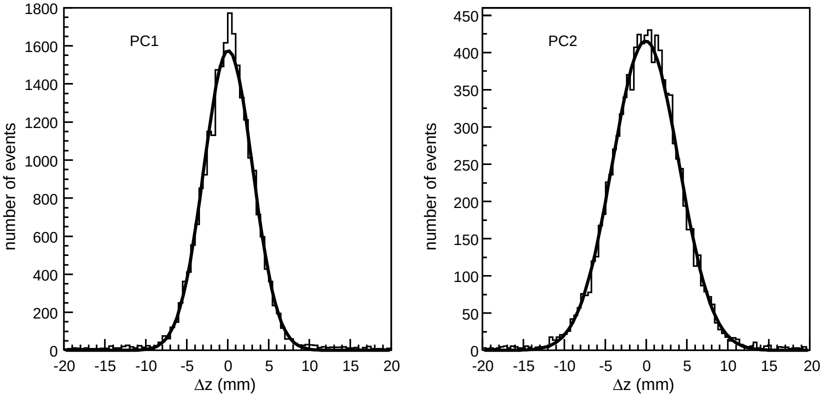

Fig. 23. Reconstructed hit position along the wire direction (z) in a PC1 and a PC2 chamber relative to the intercept of a track, projected from the center of the scintillator and the position in the reference chamber. The widths (σ_m) of the gaussian fits are 3.0 mm for PC1 and 4.1 mm for PC2.

similar to conventional wire readout, i.e. one can determine on which wire an avalanche was situated. With the pad readout, there is a complication since an unusually high charge avalanche may also fire cells that are located above the neighboring wires. In the unlikely event that this crosstalk would only be between two cells on neighboring wires, one would reconstruct this as a hit right between the two wires since this is the most probable cause of this type of 2-cell cluster. But if the cluster was due to crosstalk, one has at most made a position error equal to the wire spacing. One can reduce the crosstalk by decreasing the anode-pad distance. This reduces the extension of the induced charge on the pad plane. By choosing an anode–cathode distance of $\frac{3}{4}$ of the anode-field wire spacing, the crosstalk is a minor problem in the Pad Chambers and the position determination across the wires resembles the wire readout very well.

7. Utilities for Pad Chamber operation

7.1. High voltage system

The high voltage for a chamber is segmented into four groups with separate HV channels supply. A group contains 29 wires on PC3, 24 or 34 on PC2 and 9 or 20 on PC1. The current requirement during normal operation can be kept quite low; typically less than 100 nA for a group of anode wires. This configuration limits a possible high voltage problem to a smaller region of the chamber than if we had used a single channel for all anode wires.

The HV bus which distributes the HV to the wires has a 22 nF filter capacitor to ground, and a 10 kΩ series resistor to the bus. In order to provide noise immunity, the HV ground and detector ground are isolated through a 100 kΩ resistor. The distribution to each wire goes through a 2 MΩ resistor and a 100 pF capacitor to ground to provide an excellent charging rate without causing a HV sag during high rate operation. Should the need arise, a single wire can be removed from the HV bus by cutting the trace feeding HV to that wire.

The HV is supplied by a LeCroy 1469P module in remotely controlled LeCroy mainframes placed in racks on the spectrometer carriage. Operating voltages are 1700 V for PC1, 1840 V for PC2 and 1880 V for PC3. Trip currents during data taking are set to 10 μA for each channel controlling a group of wires, and 100 μA for the bulk supplies which feed eight channels. When turning on the

HV, the voltages are ramped up at 10 V per second, taking about 3 min to reach operating voltage. Voltages are ramped down at 100 V per second.

At the operating voltages chosen, breakdown does not occur during normal data taking. However at beam injection or when the beam is dumped, breakdown can occur due to a large number of tracks traversing at small angle relative to the wire plane. Thus, the HV is reduced to a standby voltage of 1000 V, at filling and whenever a planned dumping of beam occurs.

7.2. Low voltage system

Crates, located in racks on the movable spectrometer carriages, house the custom made low voltage supply modules. A channel in this system, provides the necessary power to one FEM. This includes three separate voltages, one for the FEM itself and two for the analog and digital parts of the ROCs. Each channel is remotely controlled and supervised through a serial bus.

Cabling between LV-supply and the FEM is an eight-conductor twelve-gauge cable. It is necessary to use such heavy gauge wire because of the long distance (approximately twenty meters) from the low voltage supply to the chambers. Although only three independent voltages are supplied, power from the most heavily loaded supply is divided between two pairs of cables to reduce resistive losses in the cable. The low voltage grounds are tied together on the FEM cards. This configuration gives the best noise immunity.

The PC1 FEMs are required to operate in a relatively high magnetic field of approximately 400 G. This necessitates an additional cable supplying a bias voltage to the differential ARCNet receivers on the FEM. PC2 and PC3 use a transformer internal to the ARCNet receiver to draw the ARCNet power from the FEM bias. This transformer would not function in the PC1 FEM location due to the residual magnetic field.

A dozen thermocouples were distributed across the PC1 FEMs and chambers, recording the temperature on the hottest part of the FEMs (voltage regulators) and at the center of the chambers themselves. During data taking these thermocouples are monitored for indications of unusual performance of the FEMs.

7.3. Gas system

The operating gas chosen for the PC is a mixture of argon and ethane in the ratio 1:1. This mixture has a long history of use in wire chambers, giving good gain with a broad safe plateau of operating voltage.

The gas sources are cryogenic liquid argon and high pressure liquid ethane. Gas from these sources are regulated to 20 psi and mixed using a Hastings Gas System Controller. Gas to each of the chambers is delivered at approximately 100 ml/min per chamber. This is verified by checking flow meters placed on the exhaust of each chamber. Needle valves on the supply pipes to the chambers allow individual flows to be adjusted, equalizing the flow through each chamber. Pressure at the chamber is typically 1 Torr above atmospheric pressure. This is maintained by placing a mineral oil bubbler in parallel with the chamber supply. If pressure at the chamber supply were to exceed 2 Torr, the bubbler would vent to the outside. In normal operation this bubbler did not bubble. Instead, the gas is returned to the mixing house where it is vented outside.

A monitoring system keeps gas flowing to the chambers within our selected operating parameters. Any fluctuations causes an alarm and a safe shutdown of the gas system, protecting the chambers and leaving the system in no danger from the flammable gas.

Gas is delivered in parallel to all chambers. The needle valves and flow meters allow us to shut off gas to an individual chamber, should the need arise, without disturbing the flow to any of the other chambers. Inside the PC1 chambers, the gas inlet is in one side of each chamber with the exhaust port on the other. This ensures that the gas is flowing throughout the entire chamber. The PC2/3 chambers have a gas inlet which travels through the S2 tube in the pixel panel and opens into the gas volume at the far end of the chamber. The exhaust ports are a pair of 1.5 mm slots which collect the gas at the near end of the chamber. This gives the best distribution of gas inside the PC2 and PC3 chambers.

The gas is delivered to the Pad Chambers through about 100 m of copper pipes. The piping was assembled primarily by soldering, with Swagelok fitting making the final connections to the chambers. The pipes were cleaned with phosphoric acid followed by rinsing with water and drying with ethanol. Moisture levels in the piping were measured to be 25 ppm after drying.

8. Summary: The first full system experience under running conditions

For the first run with the PHENIX experiment at RHIC, a large number of Pad Chambers were put in operation. In total 16 PC1 chambers (69 120 channels) and eight PC3 chambers (34 560 channels) were installed and operated. The commissioning of this system was quite straightforward and only minor problems were encountered in the chambers and the electronic readout system. Once commissioned, operation was maintained by non-expert shift personnel. The performance of the tracking system as a whole, during the first run, has been described in detail in a separate paper [15].

For the second run (2001-02), another eight PC3 chambers and eight PC2 chambers have been installed and the Pad Chamber system now comprises 172 800 channels.

Analysis of the data is in progress and all results indicate that the performance, obtained in bench tests as well as in simulations is well reproduced in the full scale system with the large multiplicity of particles passing through the chambers. The first published physics results from the PHENIX experiment, concerning the charged particle multiplicity distribution, were based on measurements with the Pad Chamber subsystem [16].

Acknowledgements

This development and construction project is a part of the PHENIX project at RHIC. The support from the PHENIX collaboration is gratefully acknowledged. We also thank the technical staffs of the participating institutions for their vital contributions. The supports from RHIC staff and the personnel in the PHENIX experimental halls are also gratefully acknowledged. We are indebted to the Vanderbilt University for providing excellent clean room facilities. The detector construction project is supported by the Department of Energy (USA), VR and the Wallenberg Foundation (Sweden), MIST and NSERC (Canada). The research was supported by Grant No. 97-00088 from the United States-Israel Binational Science Foundation (BSF), Jerusalem, Israel and by the Benoziyo Center of high energy physics at the Weizmann Institute.

References

[1] B.B. Back, et al., Phys. Rev. Lett. 87 (2001) 102303.
[2] B.B. Back, et al., Phys. Rev. Lett. 88 (2002) 022302.
[3] I.G. Bearden, et al., Phys. Rev. Lett. 88 (2002) 202301.
[4] D.P. Morrison, et al., Nucl. Phys. A 638 (1998) 565c.
[5] K. Adcox, et al., PHENIX central arm tracking detectors, Nucl. Instr. and Meth. A (2003), in press. PII: S0168-9002(02)01952-6.
[6] B. Yu, G.C. Smith, V. Radeka, E. Mathieson, IEEE Trans. Nucl. Sci. NS-38 (1991) 454.
[7] B. Yu, Ph.D. Thesis, University of Pittsburgh, Pittsburgh, 1991, pp. 69–94.
[8] L. Carlén, et al., Nucl. Instr. and Meth. A 396 (1997) 310.
[9] A. Milov et al., PHENIX technical note no. 379.
[10] Ditron S.R.L. Cerano, Italy.
[11] W.L. Bryan, et al., IEEE Trans. Nucl. Sci. NS-45 (1998) 754.
[12] M.C. Smith, et al., IEEE Trans. Nucl. Sci. NS-46 (1999) 1998.
[13] F. Sauli, CERN preprint 77-09, 1977.
[14] O. Teodorescu, Master Thesis, McGill University, Montreal, 1998.
[15] J.T. Mitchell, et al., Nucl. Instr. and Meth. A 482 (2002) 498.
[16] K. Adcox, et al., Phys. Rev. Lett. 86 (2001) 3500.